

Novel electron tomographic methods

to study the morphology of keratin filament networks

Running head: Tomography of keratin filament networks

Michaela Sailer¹, Katharina Höhn¹, Sebastian Lück², Volker Schmidt², Michael Beil³, Paul Walther¹

1. Electron Microscopy Facility, Ulm University, D-89069 Ulm, Germany

2. Institute of Stochastics, Ulm University, D-89069 Ulm, Germany

3. Department of Internal Medicine I, University Hospital Ulm, D-89070 Ulm, Germany

Correspondence to: Paul Walther, Electron Microscopy Facility, Ulm University, D-89069 Ulm, Germany; Tel: 0731/50223440, e-mail: paul.walther@uni-ulm.de

Key words: Keratin (intermediate) filaments, SEM tomography, STEM tomography, pancreas, keratin, actin, electron microscopy

Abstract

The three-dimensional keratin filament network of pancreatic carcinoma cells was investigated with different electron microscopical approaches. Semi thin sections of high-pressure frozen and freeze substituted cells were analyzed with STEM-tomography. Preservation of subcellular structures was excellent and keratin filaments could be observed, however it was impossible to three-dimensionally track the individual filaments. In order to obtain a better signal to noise ratio in transmission mode, we observed ultra thin sections of high pressure frozen and freeze substituted samples with low voltage (30 kV) STEM. Contrast was improved compared to 300 kV and individual filaments could be observed. The filament net-

work of samples prepared by detergent extraction was imaged by high resolution SEM with very good signal to noise ratio using the secondary electron signal and the three-dimensional structure could be elucidated by SEM tomography. In freeze dried samples it was possible to discern between keratin filaments and actin filaments, because the helical arrangement of actin subunits in the F-actin could be resolved. When comparing the network structures of the differently prepared samples we found no obvious differences in filament length and branching, indicating that the intermediate filament network is less susceptible to preparation artifacts than the actin network.

Introduction

Biological structures such as cytoskeletal networks are three-dimensional, classical electron microscopy, however, provides only two-dimensional images. To fill this gap, a number of techniques have been developed to record three-dimensional datasets. Although, the origins of these methods lay several decades in the past, these methods became more widely used only recently, since more efficient computer and storage devices greatly facilitate the handling of large datasets.

Three-dimensional imaging by electron microscopy

The most widely used approach to record electron tomographical datasets in a transmission type electron microscope (TEM) is tilting the sample over a large angular range of about $\pm 70^\circ$ with small increments (about 2°) and, thereby, acquiring a series of 2D projection images. This tilt series is then back-projected into a three-dimensional model (Hoppe et al., 1974 and others; recently reviewed by Baumeister, 2004). A further development of TEM tomography is scanning transmission electron microscopical (STEM) tomography (Midgley et al., 2001; Midgley & Dunin-Borkowski, 2009). Yakushevskaya et al. (2007) introduced this new technique to life science, highlighting that high angle annular dark field-STEM tomography gives

a five times better contrast and signal-to noise ratio than bright field-TEM tomography. In TEM tomography the imaging of relatively thick sections (e. g. 600 nm) suffers from inelastic scattering that blurs the image due to chromatical aberration in the projective lenses. This effect is especially pronounced at high tilt, where the path length of the electron beam in the sample increases (by about a factor of three at 70°). When a scanning beam and a STEM detector are used, however, inelastic scattering does not reduce resolution. The resolution is now mainly limited by widening of the primary beam due to scattering in the sample. Using this method with a 300 kV field emission microscope, we have been able to make tomographic reconstructions of 600 nm thick sections, in which the two leaflets of membrane lipid bilayers are still clearly resolved (Höhn et al., 2009). Thus, we considered STEM tomography a consequential method for the three-dimensional analysis of keratin filament networks. The disadvantage of using 300 kV accelerating voltage is the low contrast. We, therefore, also investigated the potential of using low voltage (30 kV) for STEM imaging (Sailer et al., 2009). Another approach with great potential for special samples is scanning electron microscopical (SEM) tomography using the secondary electron signal (Sailer et al., 2008; Lück et al., in press).

Keratin filament networks

Keratin filaments belong to the intermediate filaments, a part of the cytoskeleton, which forms a network of protein fibers in the cytoplasm of eukaryotic cells. The scaffold of the intermediate filaments defines the shape and mechanical properties of a cell (Herrmann et al., 2003), such as elasticity (Beil et al., 2003). Keratins are specifically expressed in epithelial cells and form heteropolymers of type I (K9-20) and type II (K1-8) keratin (Hatzfeld & Franke, 1985). Posttranslational modifications of keratin monomers, i.e. phosphorylation and glycosylation, regulate the solubility of keratins and thus network architecture (Coulombe & Omary, 2002; Beil et al., 2005). K8 and K18 are the basic keratins expressed in simple epithe-

lia (Fuchs & Weber, 1994) and their tumors, such as pancreatic carcinoma, which is the subject of this study.

Microscopy of keratin filament networks

Keratin filament networks have been extensively studied with light microscopical methods, with special emphasis on fluorescent microscopy. Windoffer et al. (2004) demonstrated that the keratin filament system is not homogenous but is organized into temporally and spatially distinct subdomains. They provide further evidence that continuous *de novo* formation of keratin fibers in the cell periphery is a general principle in epithelial cells. When comparing fluorescence microscopy data with electron microscopical data of the keratin filament network it is striking that the electron microscopical images contain much more structural details due to the improved resolution of the electron microscope (Fig. 1 and 2). We believe that these images reflect the complexity of eukaryotic cells that consist of about 10^{10} protein molecules of about 10^4 different kinds (Alberts et al, 2008). Unfortunately, this complexity makes life of an electron microscopist difficult, since simple and clear interpretation of the information overflow is often not possible. Electron microscopists are, therefore, seeking for strategies to make the complex relations of biological ultrastructure understandable. One of these strategies is the use of extraction protocols (Svitkina, 2007). Most of the cell compounds are, thereby, removed, and only the finely structured cytoskeleton remains. In previous studies we have analyzed the keratin network of pancreatic cancer cells using these extraction protocols. The samples have been two-dimensionally imaged in the SEM using the secondary electron signal and quantitatively analyzed by methods from spatial statistics (Beil et al. 2003, 2005 and 2006). In our recent work we have expanded these studies to visualize the three-dimensional structure of the network by SEM tomography (Sailer et al., 2008 and 2009; Lück et al., in press).

In this study we investigate and compare different preparation and imaging protocols for preservation and recording of three-dimensional keratin filament networks in pancreatic canceroid cells, including high-pressure freezing, freeze substitution, embedding and thin sectioning as well as extraction protocols. We analyzed these samples with 300 kV STEM-tomography, with (30 kV) low voltage STEM and, finally, with secondary electron SEM-tomography.

Material and Methods

Sample preparation

Cell culture

Panc 1 human pancreatic cancer cells (American Type Culture Collection, Manassas, VA, USA) were seeded (5×10^4 cells/ml) and cultivated in an incubator at 310 K and 5% CO₂. For the experiments cells were grown as a monolayer on glow discharged sapphire discs coated with carbon. (For the low voltage STEM experiments of Fig. 1E and 1F cells were grown on electron transparent carbon coated and glow discharged 200 mesh gold grids.)

Preparation of high pressure frozen and freeze substituted cells

The cells on sapphire discs were frozen using a Wohlwend HPF Compact 01 high pressure freezer (Engineering Office M. Wohlwend GmbH, Sennwald, Switzerland) as described by Buser and Walther (2008). During the following freeze substitution, water was replaced by the freeze substitution medium consisting of acetone, osmium tetroxide, uranyl acetate and 5 % of water (Walther & Ziegler, 2002). This procedure lasted about 16 - 18 hours during which the temperature was slowly increased from 183 K to 273 K. After substitution the samples were kept at room temperature for 30 minutes and then washed twice with acetone. After embedding of the samples in epon (polymerization at 333 K within 72 hours), they were cut with a microtome (Leica Ultracut UCT ultramicrotome) using a diamond knife (Diatome,

Biel, Switzerland) in ultra thin sections of a thickness of 80 nm for low voltage SEM and about 500 nm for STEM tomography and mounted on copper grids. For low voltage STEM the sections were post stained with lead citrate and uranyl acetate. Finally the samples were coated with a thin layer of carbon (5 nm) on both sides.

Preparation of extracted cells by critical point drying

In order to visualize the intermediate filament network by high-resolution SEM, a prefixation extraction method was applied, based on the protocols of Svitkina & Borisy (1998) and Svitkina (2007). After washing with phosphate-buffered saline (PBS; pH 7.3), the cells were extracted for 25 min at around 281 K with 1% Triton-X 100 (in PBS). Afterwards, cells were washed again with PBS and chemically fixed with 2.5% glutaraldehyde (in PBS and 1% saccharose) for 1 h at room temperature. After washing with PBS, the cells were contrasted with OsO₄ (2% in PBS) for 1 h at room temperature. After repeated washing with PBS, the samples were gradually dehydrated in 30%, 50%, 70%, 90%, and 100% Propanol for 5 minutes. Then the cells were critical-point dried using carbon dioxide as translation medium (Critical Point Dryer CPD 030, BalTec, Principality of Liechtenstein). Finally the samples were coated with a 5 nm layer of carbon in a freeze etching device (Baf 300, BalTec, Principality of Liechtenstein). The thickness was controlled with a quartz crystal monitor.

Preparation of extracted cells by freeze drying

Cells grown on sapphire discs were extracted with 1% Triton as described above with 10µM phalloidin added (to stabilize the actin network during preparation), and chemically fixed with 2.5% glutaraldehyde in PBS and 1% saccharose. Then they were washed with distilled water and 10 % of ethanol was added to prevent ice crystal formation during freezing. The samples were frozen by immersion in liquid propane, supercooled by liquid nitrogen. The frozen samples were mounted on a holder that fits into the Gatan cryo stage and cryo-transferred to a Baf

300 freeze-etching device (Bal-Tec, Principality of Liechtenstein). The samples were partially freeze dried for 30 min at 180 K and then for 10 min at 185 K. Finally, the samples were coated with 2 nm of tungsten by electron beam evaporation at the same temperature (Walther, 2008). The samples were never warmed up but kept cold during liquid-nitrogen transfer to the cryo-stage of the SEM.

Electron microscopy

STEM tomography

STEM tomography of semi-thin sections (500 nm) of high pressure frozen and freeze substituted Panc 1 cells was done with a Titan 80-300 field emission STEM (FEI, Eindhoven) at an accelerating voltage of 300 kV and a convergence angle of 10 mrad. Tilt series (-72° to $+72^\circ$) were recorded in scanning mode (1024 x 1024 pixels) with a high angle annular dark field detector (Fischione, Export, PA, USA). The camera length was 301 mm. Tomograms were reconstructed with the IMOD software (Kremer et al., 1996) by weighted back projection (**Figs. 1A and 1B**).

Low voltage STEM

Low voltage STEM of 80 nm ultra-thin sections of high pressure frozen and freeze substituted Panc 1 cells was performed with a cold field emission SEM (Hitachi S-5200 in-lens SEM; Tokyo, Japan) equipped with a transmission detector that was used in dark field mode for best contrast. Images (1280 x 800 pixels) were recorded in STEM mode at an accelerating voltage of 30 kV (**Figs 1C, 1D, 1E, and 5B**).

SEM tomography

SEM tomography of extracted cells was also performed with a Hitachi S-5200 in-lens SEM (Tokyo, Japan). For this purpose a holder pre-tilted by 30° was constructed which allows tilting over a range from -60° to $+60^\circ$, though the holder has to be turned by 180° and the sample needs to be remounted after recording half of the tilt series. Tomographical datasets were obtained at tilt angles from -60° to $+60^\circ$ at an increment of 2° with a magnification of 50,000 and an accelerating voltage of 5 kV using the secondary electron signal. This procedure resulted in 61 input images for the computation of a single tomogram. Tomograms were reconstructed with the IMOD software by weighted back projection. (**Figs. 3, 4, and 5A**).

Low temperature SEM of freeze dried samples

For low temperature SEM the extracted and freeze dried samples were transferred under liquid nitrogen to the cold stage (Gatan, Inc., Pleasanton, CA, U.S.A.) of the Hitachi S-5200 SEM and quickly inserted into the microscope. Specimens were investigated at a temperature of 173 K at an accelerating voltage of 30 kV using the secondary electron signal as described by Walther (2008) (**Figs. 6B and 6C**). The data are compared with a sample of in-vitro polymerized F-actin, that has been frozen, freeze dried and coated with tungsten like the samples described above (Walther, 2008) (**Fig. 6A**).

Results and Discussion

Here we present different electron microscopical approaches for the three-dimensional morphological data acquisition of keratin intermediate filament networks. In earlier work we quantitatively analyzed the keratin filament network of pancreatic cancer cells in two dimensions (Beil et al., 2005; Beil et al., 2006) and it is at hand to expand these studies to three-

dimensional datasets as we have started in Lück et al. (in press). One motivation for this study is the influence of the structure of the keratin filament network on cell mechanics, an important factor for tumor cell migration (Beil et al., 2003).

STEM tomography

In order to visualize the cytoskeleton in the full context of all cell components, we performed high pressure freezing, freeze substitution and STEM tomography. It is generally acknowledged that cryo-fixation is the best immobilization method to preserve the structural integrity of a cell (e. g. Echlin, 1992; Hohenberg et al., 2003; Dubochet, 2007). The most widely established protocol is to process a cryo-fixed sample by freeze substitution (Humbel, 2009). The samples are afterwards embedded in plastic, thin sectioned, and can be investigated by regular TEM, low voltage STEM or by (S)TEM tomography. **Fig. 1A and 1B** show virtual sections of 300 kV STEM tomograms of 500 nm sections of Panc 1 cells. **Fig. 1A** depicts the perinuclear area of a cell, where many keratin filaments are expected. Beside other well-preserved structural features such as mitochondria, densely packed filament strands are observed. It is, however, difficult to track a single filament through the whole tomogram. It is not absolutely clear, whether the observed filaments represent intermediate filaments or F-actin. **Fig. 1B** shows filaments in microvilli, which, must represent F-actin (Alberts et al., 2008).

Improvements by low voltage STEM and SEM

Since it was difficult to track the filaments with 300 kV STEM tomography, we switched to an alternative method: low voltage STEM. It is expected that contrast is enhanced at low accelerating voltages (30 kV compared to 300 kV). **Fig. 1C and 1D** are low voltage STEM dark field images of ultrathin sections from the perinuclear area of Panc 1 cells. The recorded cell area in **Fig. 1C** is similar in size to **Figs. 1A and 1B**, but the thickness of the section is only 80 nm. The contrast of the filaments is reasonably good, but obviously 3D information is

missing in the ultrathin section. Performing tomography at 30 kV is difficult with our equipment for technical reasons and, in addition we assume that spreading of the primary beam would make tomographic imaging of semi-thin sections at 30 kV unsatisfactory. Therefore, we used the extraction protocol, where most of the cellular compounds are washed out and basically only the keratin filament network remains (Svitkina & Borisy, 1998; Svitkina, 2007) unless F-actin is stabilized by adding phalloidin. **Fig. 1E and 1F** show the same area of an extracted Panc 1 cell recorded simultaneously. **Fig. 1E** is an image of the transmission dark field (STEM) signal and **Fig. 1F** is the image of the conventional secondary electron signal. The diameter of the filaments is about 10 nm in the transmitted image and about 20 nm in the secondary electron image. This is due to the carbon coat that is transparent for the transmitted electrons, but produces secondary electrons. The bright dots, which most likely represent contaminations due to incomplete extraction, are imaged with about the same contrast in both pictures, but obviously, the thin filaments are best visualized using the secondary electron signal, since they have a small volume, but a large surface area. The electrons used for contrast formation in bright field and dark field transmission imaging are scattered in function of the mass density, which is low in these thin filaments. Contrast in transmission mode is, therefore, low, and the filaments are almost vanishing beside unextracted cell compounds, which have a large volume and therefore high contrast (**Fig. 1E**). The secondary electron signal, however, is primarily a function of the surface area exposed to the electron beam (Seiler, 1967). The secondary electron emission of the filaments is high, because their surface is large compared to the volume (**Fig. 1F**). **Fig. 2A** shows an overview of an extracted Panc 1 cell imaged at an accelerating voltage of 5kV with the secondary electron signal. It turned out that in our hands an accelerating voltage of 5kV gave the best results with extracted samples at low and intermediate magnifications, since the contrast was even more increased and charging problems were reduced compared to 30kV (compare with Fig. 1F) This is in agreement with data from the literature (Pawley, 2008). The marked area is displayed at a higher magnifica-

tion in **Fig. 2B**. **Fig. 3A** represents an overview of several Panc 1 cells grown on a sapphire disc.

SEM tomography of keratin intermediate filament networks

The principle of computed tomography was first discovered by Radon (1917) in his work on the reconstruction of a function from projection data. The most essential assumption arising from this mathematical foundation of tomographic reconstruction is that the input data consists of line integrals of some image property through the volume of interest. The single projection images serving as input for reconstruction algorithms such as weighted backprojection or algebraic reconstruction techniques (Buzug, 2008) are obtained by parallel scanning of the sample with a line while taking the integrals. The Radon transform of an object is the collection of these projections which is obtained by tilting the sample in the interval $[-90^\circ, +90^\circ]$ with respect to a central axis. Computed tomography deals with the problem of inverting the Radon transform.

At the level of resolution needed to study keratin networks the signal collected in STEM mode by a high angular dark field detector can be directly related to the projection of the density through the specimen along the path of the electron beam, thus approximating line integration by an integral over the electron probe (Hawkes, 2005). However, the secondary electron signal recorded as the input data for SEM tomograms is of quite different nature. The escape probability of secondary electrons decreases exponentially with the depth of the location where the secondary electron is generated (Goldstein et al., 2007). Therefore, the secondary electron signal primarily maps surfaces and contains a rather negligible amount of information on deeper layers of the specimen. As a consequence, in usual situations secondary electron imaging does not yield projections of the specimen which could be used as input for tomographic reconstruction algorithms. However, detergent extracted samples of keratin fila-

ments only contain the fine network structure surrounded by vacuum. As a consequence, single surface locations along the filaments are freely accessible to the electron probe under most tilt angles. Thus, even under high tilt angles filaments in deeper areas are clearly visible (**Fig. 3C and 3D**) and the secondary electron signal closely resembles projection data of the specimen. Compared to real projection data the contrast of filaments in lower network components is decreased by shadowing effects of network parts (**Fig. 3C**). In comparison to STEM the crucial advantage of secondary electron imaging is the enhanced contrast of the filaments (**Fig. 1E vs. 1F**). This high contrast got transferred to tomograms computed from secondary electron tilt series, which were recorded by tilting in the interval $[-60^\circ, 60^\circ]$ at an angular increment of 2° and computed by weighted backprojection (Buzug, 2008) (**Fig. 4A**). Thus the tomograms were generated by a standard algorithm for the reconstruction of TEM or STEM data.

A specific artifact in SEM tomograms is that shadowing of filaments in deeper layers by upper network components decreases contrast and leads to stretched filament profiles. The oval stretch of reconstructed filament profiles in SEM tomograms is a well-known artifact from tomographic reconstructions with a missing wedge of tilt angles, which also occurs in computed tomography from regular TEM tilt series (Midgley & Dunin-Borkowski, 2009). However, in SEM tomograms these effects are more pronounced due to mutual shadowing of the image components. As a consequence, SEM tomography for the 3D analysis of filamentous networks is not primarily limited by sample thickness but by network density, which controls visibility of single filaments during tilting. For more details we refer to Lück et al. (in press).

Quantitative analysis of network structure based on SEM tomograms

Based on high contrast SEM tomograms the graph structure of the networks can be extracted by techniques from image analysis. **Fig. 4B** depicts the tomogram after thresholding. **Figs. 4C and D** visualize the network graph extracted from the thresholded tomogram by means of an algorithm discussed in Lück et al. (in press). Apart from the segmentation of the foreground phase by thresholding, the algorithm applied to generate **Fig. 4C and D** is fully automatic and thus reduces potential bias from user interaction. Given the extracted network graph, statistical analysis of network characteristics such as network density, filament length, and cross-link topology can be conducted. Since such characteristics are related to the mechanical behavior of the network, these techniques represent promising approaches to quantitatively link network morphology to mechanical properties of the cytoplasm and the migration ability of cells, which can be measured in biophysical experiments (Marti et al, 2008; Lautenschläger et al., 2009).

Preparation artifacts

Possible artifact formation of extraction and critical point drying protocols have been described in the literature, such as surface tension artifacts caused by traces of water during critical point drying (Ris, 1985) as well as fracturing of actin filaments, leading to branch-like structures (Resch et al., 2002; Vignal & Resch, 2003). In order to obtain more confidence in our preparation protocol, we compared extracted samples with the results of freeze substitution (Fig. 5) and freeze drying experiments (Fig. 6).

In Fig. 5 we compare two different preparation and visualization methods for a similar volume in a Panc 1 cell. Fig. 5A is an artificially generated section (about 80 nm) of tomogram PP2 (the sample was detergent extracted), whereas Fig. 5B is an image of an ultra thin section (thickness about 80 nm) of a high pressure frozen and freeze substituted Panc 1 cell. Both

images, therefore, represent the same surface area and the same thickness after different preparation and visualization methods. Taking into account that the filaments appear thicker in the secondary electron SEM image (Fig. 5 A) due to the carbon coating, as explained above, both images show similar variation of filament density. Moreover, under both preparation methods the filaments form rather long tracks, which are partially organized in parallel strands. We conclude, therefore, that fracturing of filaments as postulated by Resch et al. (2002) for F-actin in critical point dried samples does not occur in these intermediate filament samples.

In Fig. 6 we compared our results for critical point dried samples with freeze dried controls. We added phalloidin to the extraction medium in order to better preserve the actin filament structure. As described earlier (Walther, 2003 and 2008) the helical arrangement of individual actin subunits is well visible in isolated actin filaments after freeze drying and coating with a very thin layer of tungsten (Fig. 6A), but not after critical point drying. Fig. 6B and 6C show different areas from the same extracted and freeze dried Panc 1 cell preparation. Fig. 6B is from the cell periphery where mainly actin filaments are expected, and, indeed, we find saw tooth-like surface structures on most of the filaments in this area. Fig. 6C is from a perinuclear area, where we mainly expect keratin (intermediate) filaments. In fact, most of the filaments in this image show a smooth appearance.

Fig. 6D and 6E show SEM images of freeze dried (Fig. 6D) and critical point dried (Fig. 6E) networks. Comparing central regions after freeze drying (Fig. 6D) and after critical point drying (Fig. 6E) the keratin filament network appeared similar after both preparations and, most notably, we could not observe more branching in critical point dried samples. Based on these results we suppose that the keratin filament network is more stable than the actin network and,

therefore, less affected by chemical and mechanical disturbance during extraction, fixation, dehydration and drying.

Conclusions:

In an earlier work (Lück et al., in press), we performed statistical analysis of three-dimensional keratin filament networks. These samples had been prepared by the extraction protocol combined with critical point drying and imaged by SEM tomography. These techniques yield a high level of contrast in tomograms, which is necessary for the extraction and analysis of the network structure by means of image analysis and spatial statistics, but cannot be achieved by the other methods discussed in the present study. Here we confirmed that the network structure of keratin (intermediate) filaments appears similar after being prepared by different preparation protocols. This gives confidence that the three dimensional structure of the network is well preserved by all of the different preparation protocols used in this work, including SEM tomography of extracted cells.

Acknowledgment

We thank Renate Kunz, Elke Wolff-Hieber, Eberhard Schmid and Reinhard Weih for excellent technical assistance. We thank Guido Adler for continuous support. This work was supported by the DFG SFB 518, project B21 and B22.

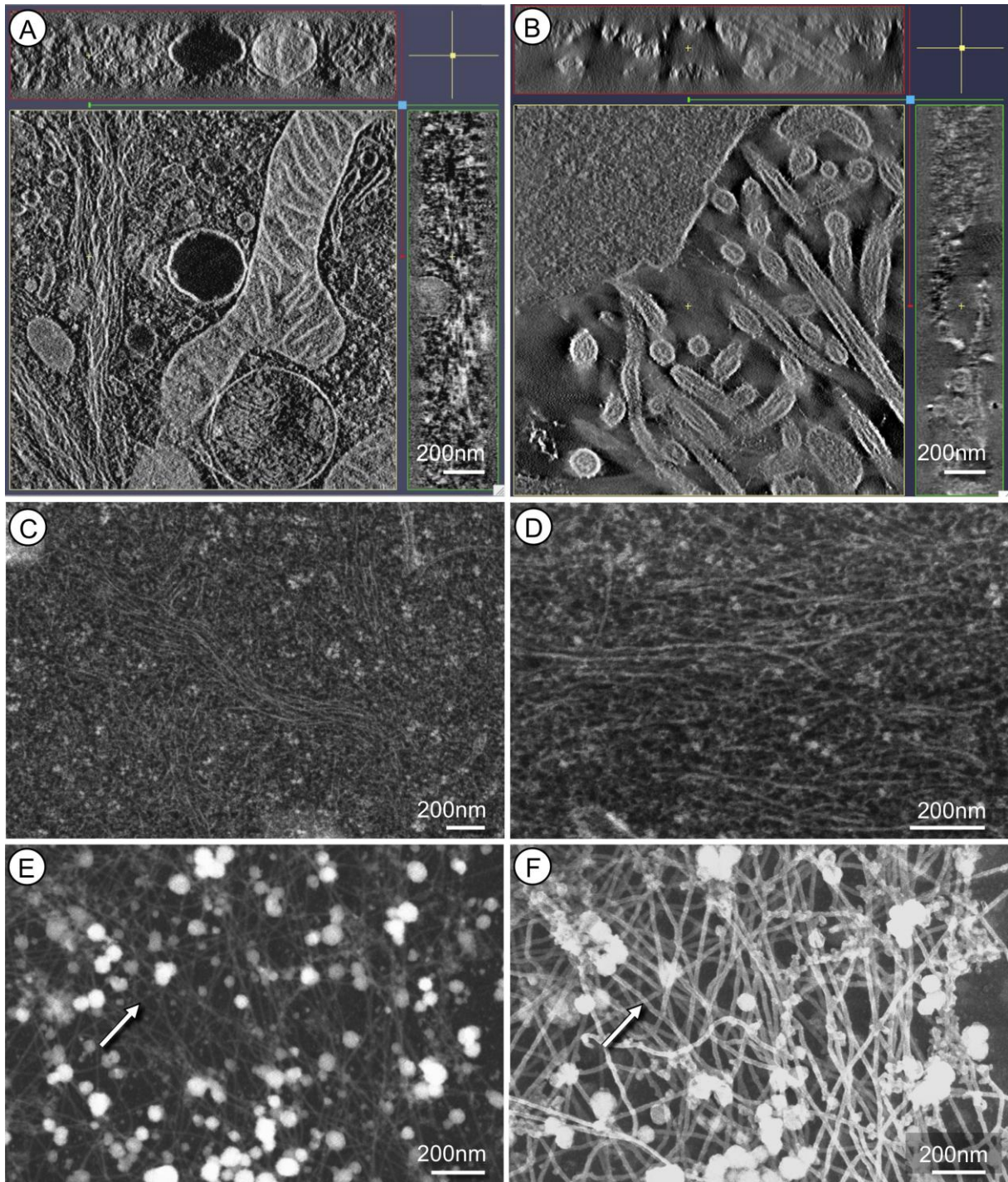


Fig. 1 **A** as well as **B** show computed sections of 300 kV STEM tomograms of high pressure frozen and freeze substituted Panc 1 cells. **1A** was recorded in the perinuclear area whereas **1B** represents a peripheral area of a cell. **1C** and **1D** are thin sections (80 nm) recorded with an SEM at 30 kV with a dark field STEM detector. The contrast of the filaments is reasonably good, but obviously 3D information is missing. **1E** and **1F** show the same area of an extracted Panc 1 cell imaged simultaneously in an SEM at 30 kV. **1E** was recorded using the transmission dark field signal whereas **1F** is the image of the secondary electron signal. The contrast of the thin filaments is considerably higher in the secondary electron image (**1F**) than in the transmission image (**1E**). Arrows depict the same filament.

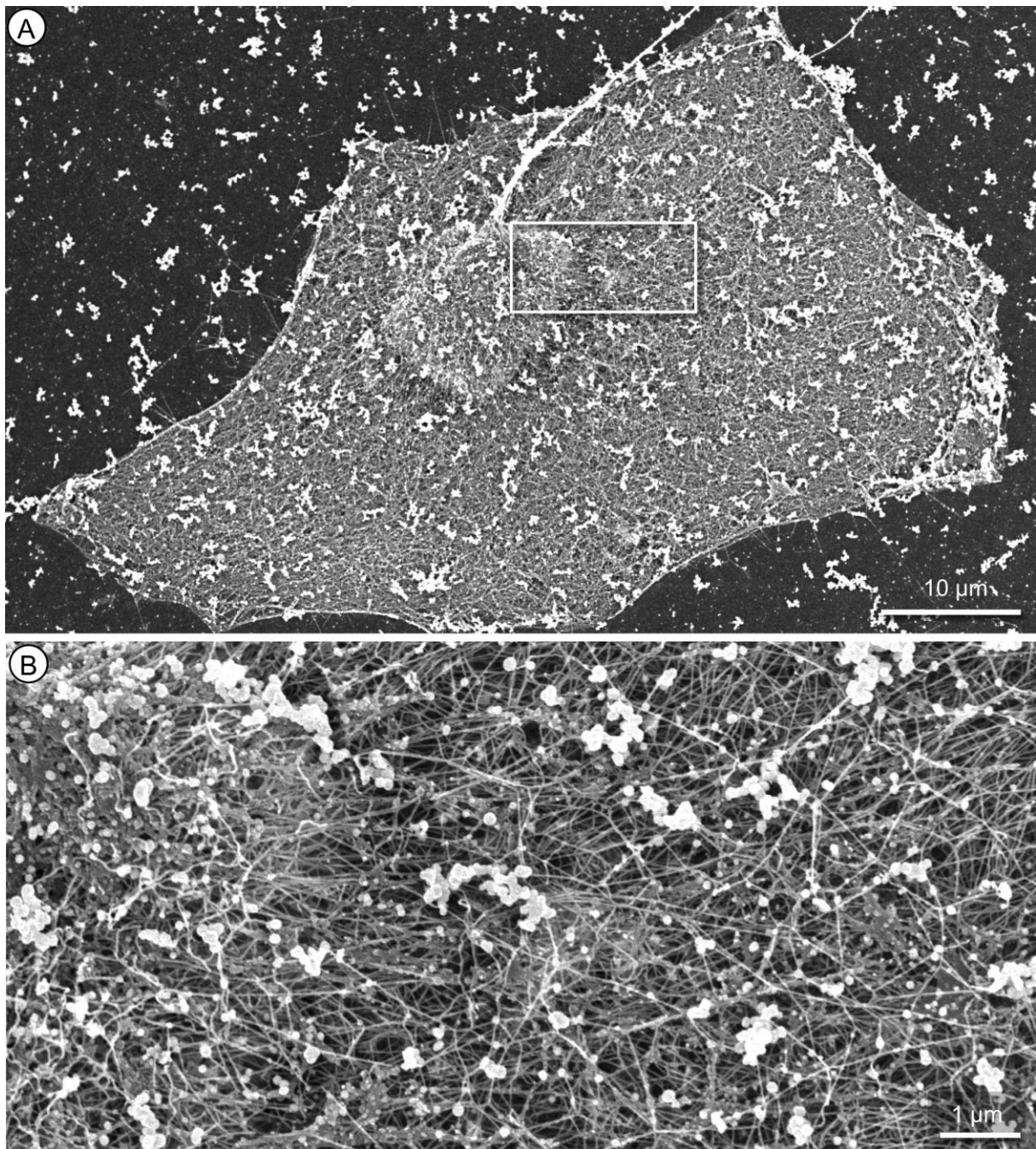


Fig. 2A shows an overview of an extracted Panc 1 cell. The rectangular marked area is displayed at higher magnification in **2B**. These cells exhibit an extremely complex and dense filament network. Some agglomerated cell components are still left, since they were not completely removed during extraction. Both images were recorded with an SEM at 5 kV using the secondary electron signal.

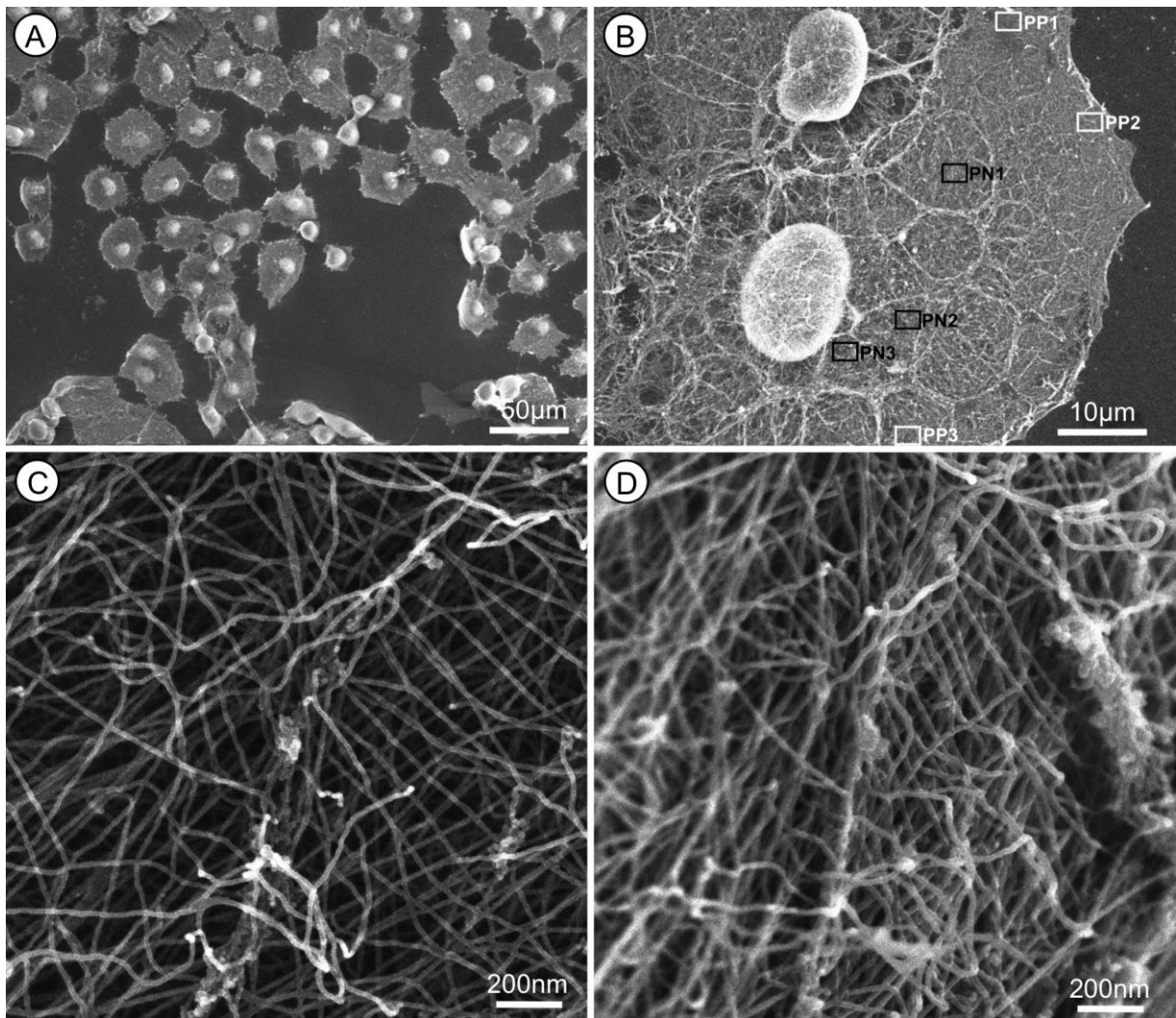


Fig. 3A represents an overview of extracted Panc 1 cells. **Fig. 3B** shows a cell where several tomograms were recorded at different perinuclear (PN, black boxes) and peripheral (PP, white boxes) areas. **3C** and **3D** show images at 0° tilt angle (**3C**) and at 60° tilt angle (**3D**) of the recorded tilt series (-60° - +60°; 2° steps) of tomogram PP2 in **Fig. B**. All images were recorded with an SEM at 5 kV using the secondary electron signal.

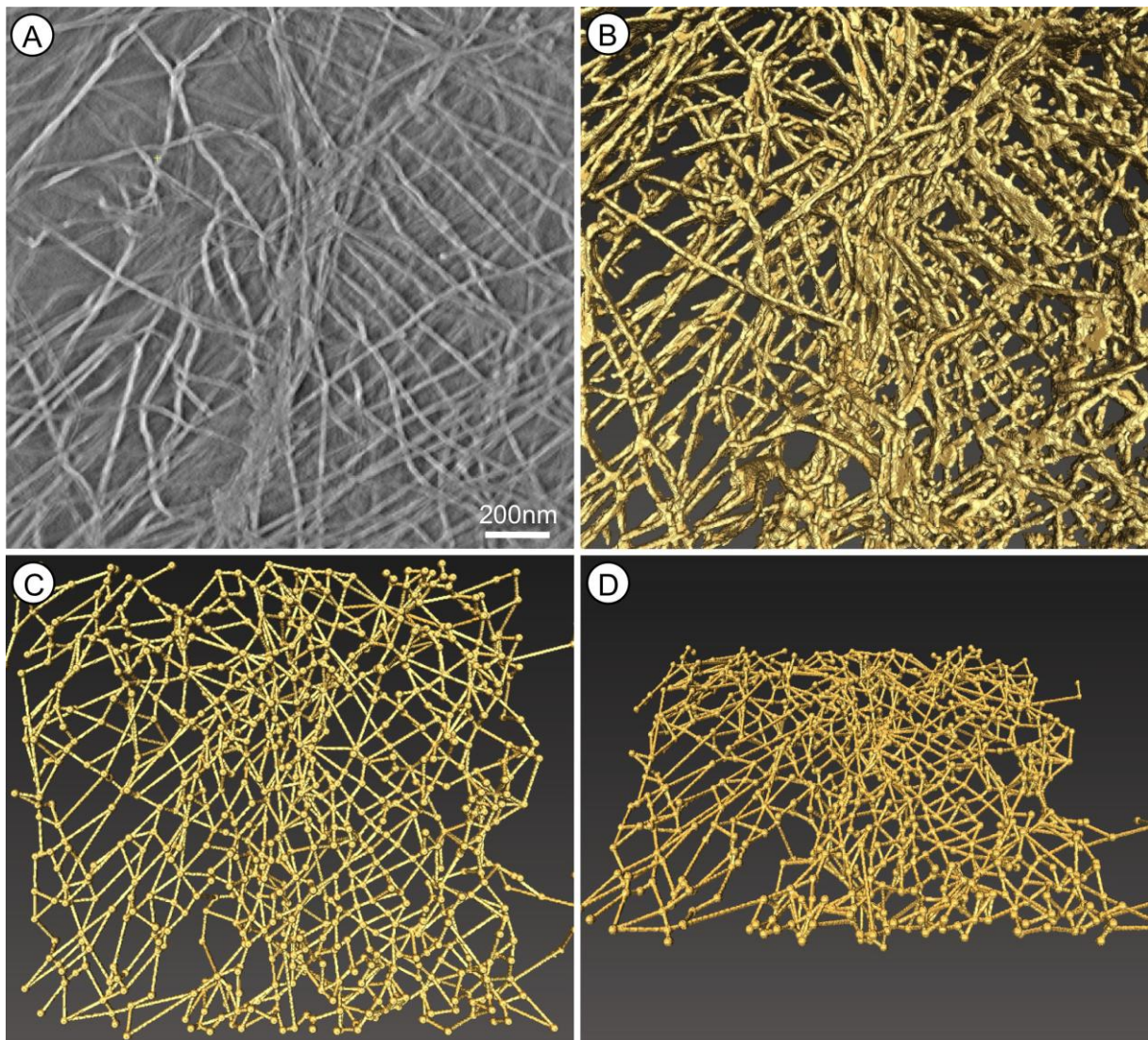


Fig. 4A shows one layer of a reconstructed tomogram of the region PP2 in Fig. 3B. Fig. 4B depicts the tomogram after thresholding. Figs. 4C and 4D represent the network graph calculated from the thresholded tomogram, visualized under different tilt angles.

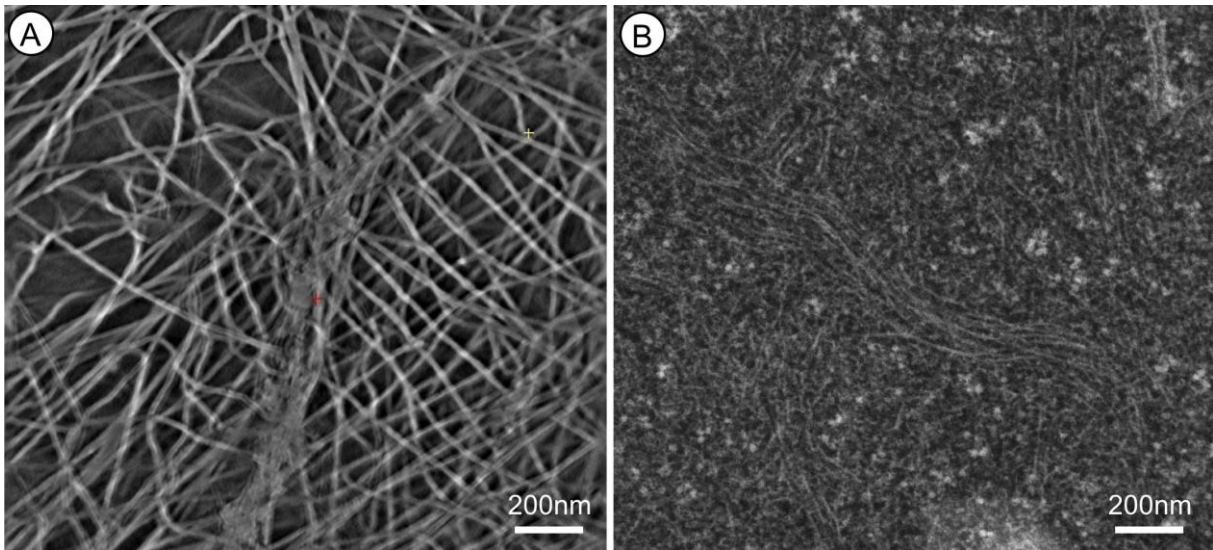


Fig. 5A is an artificially generated section (about 80 nm thick) of tomogram PP2, from a detergent extracted and critical point dried sample. **Fig. 5B** is an image of an ultra thin section (thickness about 80 nm) of a high pressure frozen and freeze substituted Panc 1 cell, imaged with an SEM at 30 kV with a dark field STEM detector. Both images visualize the same field size and the same thickness after different preparation and visualization methods. The filaments in the secondary electron SEM image (**Fig. 5A**) appear thicker than the ones in the transmission electron image (**Fig. 5B**). This is due to carbon coating, as explained in **Fig. 1E**. Besides this difference, both images show similar appearance of the filaments.

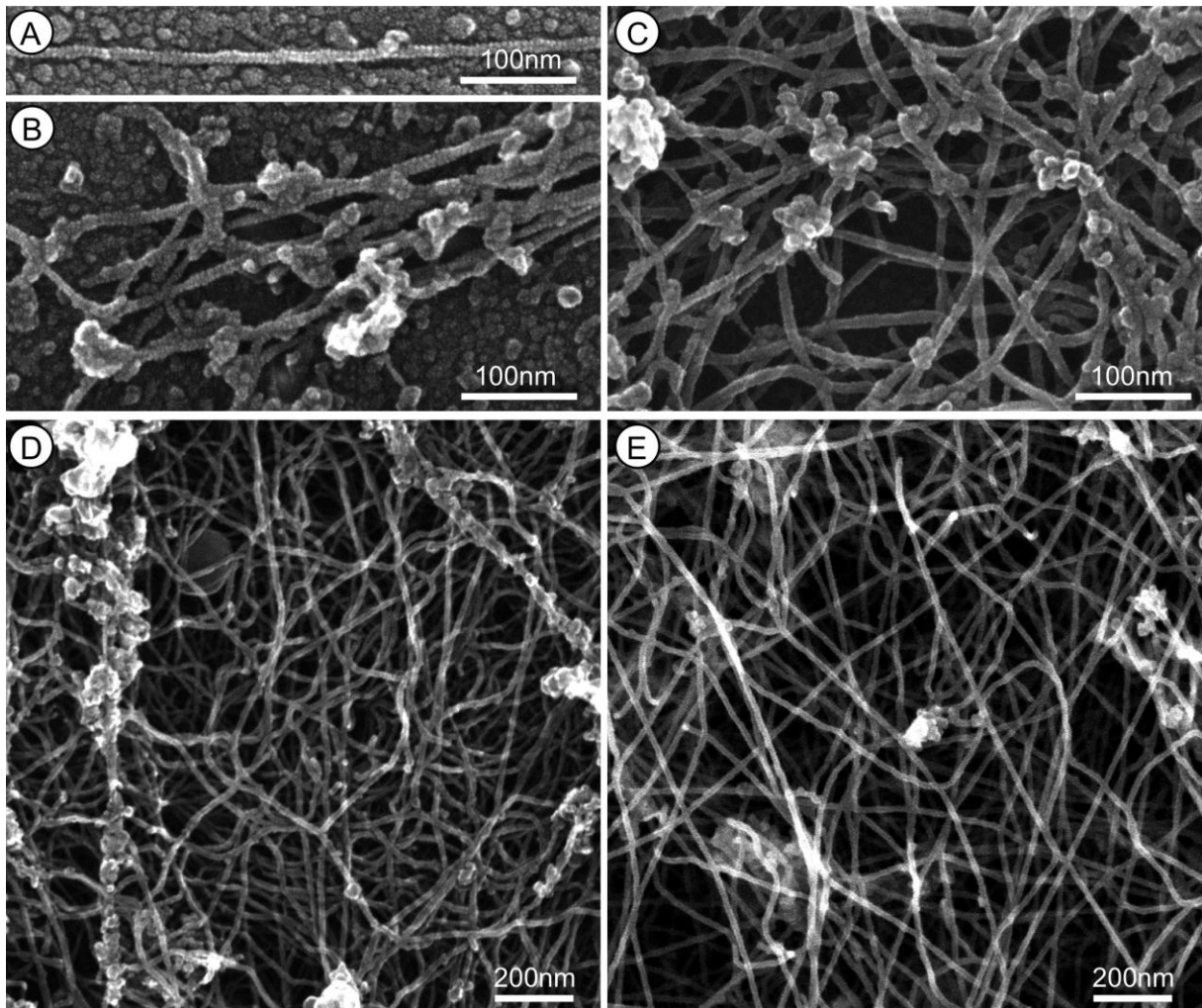


Fig. 6A shows an isolated actin filament after freeze drying. The typical helical arrangement of the individual G-actin subunits can be seen clearly and give the filament the typical saw tooth like appearance. **Fig. 6B and 6C** are different areas from the same extracted Panc 1 cell preparation after freeze drying. **Fig. 6B** is from the cell periphery, where mainly actin filaments are expected. Indeed, most of the filaments in this area exhibit saw tooth-like surface structures. **Fig. 6C** is from a perinuclear area, where we mainly expect keratin (intermediate) filaments. Most of the filaments show a smooth appearance. **Fig. 6D and 6E** show SEM images of freeze dried (**Fig. 6D**) and critical point dried (**Fig. 6E**) extracted networks. Both images show similar branching and directional distribution of the filaments. All images were recorded with an SEM using the secondary electron signal.

References

- Alberts, B., Johnson, A., Lewis, L., Raff, M., Roberts, K. & Walter, P. (2008) *Molecular Biology of the Cell*, fifth edition. Garland Publishing, New York, NY.
- Baumeister, W. (2004). Mapping molecular landscapes inside cells. *Biol Chem* **385**, 865–872.
- Beil, M., Micoulet, A., von Wichert, G., Paschke, S., Walther, P., Omary, M.B., Van Veldhoven, P.P., Gern, U., Wolff-Hieber, E., Eggermann, J., Waltenberger, J., Adler, G., Spatz, J. & Seufferlein, T. (2003). Sphingosylphosphorylcholine regulates keratin network architecture and visco-elastic properties of human cancer cells. *Nat Cell Biol* **5**, 803-811.
- Beil, M., Braxmeier, H., Fleischer, F., Schmidt, V. & Walther, P. (2005). Quantitative analysis of keratin filament networks in scanning electron microscopy images of cancer cells. *J Microsc* **220**, 84-95.
- Beil, M., Eckel, S., Fleischer, F., Schmidt, H., Schmidt, V. & Walther, P. (2006). Fitting of random tessellation models to keratin filament networks. *J Theor Biol* **241**, 62-72.
- Buser, C. & Walther, P. (2008). Freeze-Substitution: The addition of water to polar solvents enhances the retention of structure and acts at temperatures around $-60\text{ }^{\circ}\text{C}$. *J Microsc* **230**, 268-77.
- Buzug, T.M. (2008). *Computed Tomography*. Springer, Berlin.

Coulombe, P.A. & Omary, M.B. (2002). 'Hard' and 'soft' principles defining the structure, function and regulation of keratin intermediate filaments. *Curr Opin Cell Biol* **14**, 110-22.

Dubochet, J. (2007). The physics of rapid cooling and its implications for cryoimmobilization of cells. *Methods Cell Biol* **79**, 7-21.

Echlin, P. (1992). *Low-Temperature Microscopy and Analysis*. Plenum Press, New York and London.

Fuchs, E. & Weber, K. (1994). Keratin (intermediate) filaments: structure, dynamics, function and disease. *Annu Rev Biochem* **63**, 345-82.

Goldstein, J., Newbury, D., Joy, D., Lyman, C., Echlin, P., Lifshin, E., Sawyer, L. & Michael, J. (2007). *Scanning Electron Microscopy and X-Ray Microanalysis*, third edition. Springer, New-York.

Hatzfeld, M. & Franke, W.W. (1985). Pair formation and promiscuity of cytokeratins: formation in vitro of heterotypic complexes and keratin (intermediate)-sized filaments by homologous and heterologous recombinations of purified polypeptides. *J Cell Biol* **101**, 1826-41.

Hawkes, P.W. (2005). The electron microscope as a structure projector. In: J. Frank (Ed.), *Electron Tomography*, second edition, pp.83-107. Springer-Verlag New-York.

Herrmann, H., Hesse, M., Reichenzeller, M., Aebi, U. & Magin, T.M. (2003). Functional complexity of keratin (intermediate) filament cytoskeletons: from structure to assembly to gene ablation. *Int Rev Cytol* **223**, 83-175.

Hohenberg, H.H., Müller-Reichert, T., Schwarz, H. & Zierold, K. (2003). Foreword, Special Issue on High Pressure Freezing. *J Microsc* **212**, 1-2.

Höhn, K., Pusapati G.V., Seufferlein T., Adler G. & Walther, P. (2009). 3D reconstruction of Golgi stacks in Brefeldin A treated cells. First results using STEM tomography. In: M.A. Pabst and G. Zellnig (Eds), *Proceedings of MC2009*, Vol. 2 Life Science pp. 43-44. Verlag der TU Graz.

Hoppe, W., Gassmann, J., Hunsmann, N., Schramm, H.J. & Sturm, M. (1974). Three-dimensional reconstruction of individual negatively stained yeast fatty-acid synthetase molecules from tilt series in the electron microscope. *Z Physiol Chem* **355**, 1483-1487.

Humbel, B.M. (2009). Freeze Substitution. In: Cavalier, A., Spohner, D., and Humbel, B.M. (Eds.), *Handbook of cryo-preparation methods for electron microscopy*, pp. 319-341. CRC Press, Boca Raton.

Kremer, J.R., Mastrorade, D.N. & McIntosh, J.R. (1996). Computer visualization of three-dimensional image data using IMOD. *J Struct Biol* **116**, 71-76.

Lautenschläger, F., Paschke, S., Schinkinger, S., Bruel, A., Beil, M. & Guck, J. (2009). The regulatory role of cell mechanics for migration of differentiating myeloid cells. *Proc Natl Acad Sci U S A*. **106**, 15696-15701.

Lück, S., Sailer, M., Schmidt, V. & Walther, P. Three-dimensional analysis of intermediate filament networks using SEM-tomography. *J. Microsc.* in press, doi: 10.1111/j.1365-2818.2009.03348.x.

Marti, O, Holzwarth, M. & Beil, M. (2008). Measuring the nanomechanical properties of cancer cells by digital pulsed force mode imaging. *Nanotechnology* **19**, 384015.

Midgley, P.A., Weyland, M., Thomas, J. M., Johnson, B.F.G. (2001). Z-contrast tomography: A technique in 3-dimensional nanostructural analysis based on Rutherford scattering. *Chem Comm* **18**, 907-908.

Midgley, P.A. & Dunin-Borkowski, R.E. (2009). Electron tomography and holography in materials science. *Nat Mater* **8**, 271-280.

Pawley, J. (2008). LVSEM for Biology. In: Schatten H, Pawley J.B. (eds) *Biological Low-Voltage Scanning Electron Microscopy*. pp 27-106. Springer New York.

Radon, J. (1917). Über die Bestimmung von Funktionen längs gewisser Mannigfaltigkeiten. *Berichte der math.-phys. Kl. Sächsischen Gesellschaft der Wissenschaften* **59**, 262–77.

Resch, G.P., Goldie, K.N., Krebs, A., Hoenger, A. & Small, J.V. (2002). Visualisation of the actin cytoskeleton by cryo-electron microscopy. *J Cell Sci* **115**, 1877-1882.

Ris, H. (1985). The Cytoplasmic Filament System in Critical Point-dried Whole Mounts and Plastic-Embedded Sections. *J Cell Biol* **100**, 1474-1487.

Sailer, M., Lück, S., Schmidt, V., Beil, M., Adler, G. & Walther, P. (2008). Three-dimensional analysis of the keratin (intermediate) filament network using SEM-tomography. In: A. Aretz, B. Hermanns-Sachweh, J. Mayer (Eds.), *Proceedings of EMC 2008*, pp. 91-92. Springer-Verlag Berlin Heidelberg.

Sailer, M., Lück, S., Schmidt, V., Beil, M., Adler, G. & Walther, P. (2009). Three-dimensional analysis of the keratin (intermediate) filament network using SEM-tomography. In: M.A. Pabst and G. Zellnig (Eds), *Proceedings of MC2009*, pp. LI.P603-604. Verlag der TU Graz.

Seiler, H. (1967). Einige aktuelle Probleme der Sekundärelektronenemission. *Z angew Phy* **22**, 249-263.

Svitkina, T.M. (2007) Electron microscopic analysis of the leading edge in migrating cells. *Methods Cell Biol* **79**, 295-319.

Svitkina, T.M. & Borisy, G.G. (1998). Correlative light and electron microscopy of the cytoskeleton of cultured cells. *Method Enzymol* **298**, 570-592.

Vignal, E. & Resch, G. (2003). Shedding light and electrons on the lamellipodium: imaging the motor of crawling cells. *Biotechniques* **34**, 780-4, 786, 788-9

Walther, P. & Ziegler, A. (2002), Freeze substitution of high-pressure frozen samples: the visibility of biological membranes is improved when the substitution medium contains water. *J Microsc* **208**, 3-10.

Walther, P. (2003). The potential of high resolution cryo-SEM in life science. *Hitachi Instrument News* **40**, 3-8.

Walther, P. (2008). High-resolution cryo-SEM allows direct identification of F-actin at the inner nuclear membrane of *Xenopus* oocytes by virtue of its structural features. *J Microsc* **232**, 379-85.

Windoffer, R., Wöll, S., Strnad, P. & Leube, R.E. (2004). Identification of novel principles of keratin filament network turnover in living cells. *Mol Biol Cell* **5**, 2436-48.

Yakushevskaya, A.E., Lebbink, M.N., Geerts, W.J., Spek, L., van Donselaar, E.G., Jansen, K.A., Humbel, B.M., Post, J.A., Verkleij, A.J., Koster, A.J. (2007). STEM tomography in cell biology. *J Struct Biol* **159**, 381-391.